I-Chen Lin (✉)
Ming Ouhyoung

Mirror MoCap: Automatic and efficient capture of dense 3D facial motion parameters from video

I-C. Lin
Dept. of Computer and Information
Science, National Chiao Tung University,
1001 Ta Hsueh Road, Hsinchu, 300,
Taiwan
e-mail: ichenlin@cis.nctu.edu.tw

M. Ouhyoung
Dept. of Computer Science and
Information Engineering, National Taiwan
University, No.1 Roosevelt Rd. Sec. 4,
Taipei, 106, Taiwan
e-mail: ming@csie.ntu.edu.tw

Abstract In this paper, we present an automatic and efficient approach to the capture of dense facial motion parameters, which extends our previous work of 3D reconstruction from mirror-reflected multiview video. To narrow search space and rapidly generate 3D candidate position lists, we apply mirrored-epipolar bands. For automatic tracking, we utilize spatial proximity of facial surfaces and temporal coherence to find the best trajectories and rectify statuses of missing and false tracking. More than 300 markers on a subject's face are tracked from video at a process speed of 9.2 frames per second (fps) on a regular PC. The estimated 3D facial motion trajectories have been applied to our facial animation system and can be used for facial motion analysis.

1 Introduction

From a big smile to a subtle frown to a pursed mouth, a face can perform various kinds of expressions to implicitly reveal one's emotions and meanings. However, these frequent expressions, which we usually take for granted, involve highly complex internal kinematics and sophisticated variations in appearance. For example, during pronunciation, nonlinear transitions of a face surface depend on preceding and successive articulations, a phenomenon known as coarticulation effects [10].

In order to comprehend the complicated variations of a face, recently more and more researchers have been using motion capture techniques that simultaneously record 3D motion of a large number of sensors. When sensors are placed on a subject's face, these techniques can extract the approximate motion of these designated points. Today, commercial motion capture devices, such as optical or optoelectronic systems, are able to accurately track dozens of sensors on a face. However, these devices are usually very expensive, and the expense becomes a significant barrier for researchers intending to devote themselves to areas related to facial analysis. Moreover, current motion capture devices are unable to track spatially dense facial sensors without interference. Not only can a large quantity of facial motion parameters directly provide more realistic surface deformation for facial animation, but the dense facial motion data could also be a key catalyst for further research. From the aspect of face synthesis, in the current process of animation production, facial motion capture data of 20 to 30 feature points are used to drive a well-prepared synthetic head. Motion vectors on the face's uncovered areas are estimated by internal virtual muscles, scattering functions, or surface patches. Animators can only adjust coefficients of the muscles or patches empirically from their observations. With dense facial motion data as criteria, the coefficients can be automatically calculated, and the results will be more faithful to real human facial expression. Regarding facial analysis, numerous hypotheses or models have been proposed to simulate facial motion and kinematics. Most current research uses only sparse facial feature points [18, 19] due to tracking device capacities. Sizeable and dense facial mo-

tion trajectories can provide further detailed information for correlations of facial surface points in visual speech analysis.

In our previous work [20], we proposed an accurate 3D reconstruction algorithm for mirror-reflected multiview images and a semiautomatic 3D facial motion tracking procedure. Our previous system can track around 50 facial markers using a single video camcorder with two mirrors under normal light conditions. When tracking dense facial markers, we found that ambiguity in block matching caused the tracking to degenerate dramatically. Occlusion is the most critical problem: for example, when our mouths are pouting or opened wide, the markers below the lower lips vanish in video clips. We tried to use thresholding in block matching and Kalman predictors to tackle this problem; despite our efforts, it works satisfactorily only for short-term marker occlusion.

Fully automatic tracking of multiple target trajectories over time is called the "multitarget tracking problem" in radar surveillance systems [8]. When only affected by measurement error and false detection, this problem is equivalent to the minimum cost network flow (MCNF) problem. The optimal solution is efficient [9, 27]. Nevertheless, when measurement errors, missing detection (false negative), and false alarms (false positive) all occur during tracking, time-consuming dynamic programming is required to estimate approximate trajectories, and the tracking results can degenerate seriously even if the occurrence frequency of missing detection slightly increases [28]. In our experiments, even though fluorescent markers and blacklight lamps are used to enhance the clarity of markers and to improve the steadiness of markers' projected colors, missing and false detections are still unavoidable in the feature extracting process.

Fortunately, the motion of markers on a facial surface is unlike that of targets tracked in radar systems. Targets in the general multitarget-tracking problem move independently, and consequently the judgement of a target's best trajectory can only stand on its prior trajectory. In contrast, points on a facial surface have not only temporal continuity but also spatial coherence. Except for the mouth, nostrils, and eyelids, a face is mostly a continuous surface, and a facial point's positions and movements are similar to those of its neighbors. With this additional property, automatic diagnoses of missing and false detection become feasible and the computation is more efficient.

Guenter et al. [14] tracked 182 dot markers painted with fluorescent pigments for near-UV light. This research used special markers and lights to enhance the feature detection, and the researchers took into account the spatial and temporal consistency for reliable tracking. Guenter and his colleagues' impressive work inspired us.

In this proposed work, we follow our previous framework of estimating 3D positions from mirror-reflected multiview video clips [20] in which two mirrors are placed near a subject's face and a single video camera is used to record simultaneously frontal and mirrored facial images. Instead of normal light conditions, to improve clarity, we also apply markers with UV-responsive pigments for blacklight blue (BLB) fluorescent lights. Compared to Guenter et al.'s work, the proposed method is more efficient and versatile.

Guenter et al.'s work required subjects' heads to be immobile because of the limitation of markers' vertical orders in their marker matching routine, and therefore head movement had to be tracked independently by other devices. In addition, there was no explicit definition of tracking errors in this method, and an iterative approach was used for node matching. In contrast, our proposed method is capable of automatically tracking both facial expressions and head motions simultaneously without synchronization problems. Furthermore, we propose using mirrored epipolar bands to rapidly generate 3D candidate points from projections of extracted markers and forming the tracking as a node-connection problem. Both spatial and temporal coherence of dense markers' motion are applied to efficiently detect and compensate missing tracking, false tracking, and tracking conflicts. Our system is now able to capture more than 300 markers at a process speed of 9.2 fps and can be extended for a regular PC to track more than 100 markers from live video in real time.

This paper is organized as follows. In Sect. 2, we mention related research in facial motion capture and face synthesis. Section 3 describes equipment setting and gives an overview of our proposed tracking procedure. Section 4 presents how to extract feature points from image sequences and explains the construction of 3D candidates. In Sect. 5, we present a procedure to find the best trajectories and to tackle the problem of missing and false tracking. The experimental results and discussion are presented in Sect. 6. Finally, we present our conclusions in Sect. 7.

2 Related work

For tracking to be fully automatic, some studies have employed a generic facial motion model. Goto et al. [13] used separate simple tracking rules for eyes, lips, and other facial features. Pighin et al. [23, 24] proposed tracking animation-purposed facial motion based on linear combination of 3D face model bases. Ahlberg [1] proposed a near-real-time face tracking system without markers or initialization. In "voice puppetry" [7], Brand applied a generic head mesh with 26 feature points, where spring tensions were assigned to each edge connection. Such a generic facial motion model can rectify "derailing" trajectories and is beneficial for sparse feature tracking; however, an approximate model can also overrestrict the feature tracking while a subject does exaggerated or unusual facial expressions.
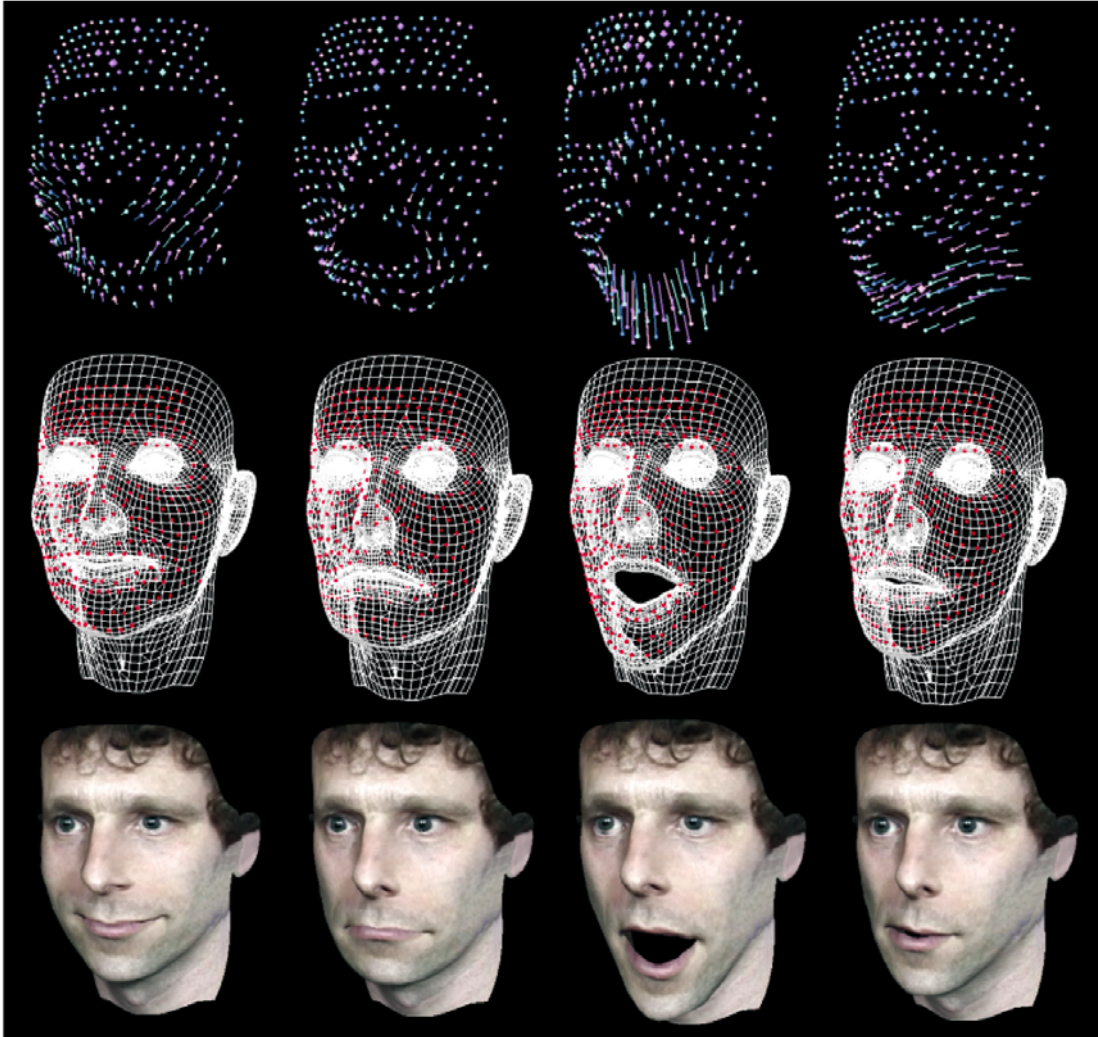
Fig. 1. Applying extracted motion parameters of 300 markers to a sythetic face. The first row is extracted 3D motion vectors where the line segments represent displacement comparing to the neutral face; the middle row is a generic head driven by retargeting motion data; in the third row, the retargeting motion data are applied to a personalized face

For 3D facial motion tracking from multiple cameras, an optoelectronic system, e.g., Optotrak (`www.ndigital.com/optotrak.html`), uses optoelectronic cameras to track infrared-emitting photodiodes on a subject's face. This kind of instrument is highly accurate and appropriate for analysis of facial biomechanics or coarticulation effects. However, each diode needs to be powered by wires, which may interfere with a subject's facial motion.

Applying passive markers can avoid this problem. In the computer graphics industry for movies or video games, animators usually make use of protruding spherical markers with high response to a special spectrum band, e.g., red visible light or infrared in the vicon series (`www.vicon.com`). The high response and spherical shape make feature extraction and shape analysis easier, but these markers do not work well for lip surface motion tracking because people sometimes tuck in their lips, and these markers will obstruct the motion. Besides, the extracted motion of protruding markers is not the exact motion on a face surface but the motion at a small distance above the surface.

In addition to capturing stereo videos with multiple cameras, Patterson et al. [22] proposed using mirrors to acquire multiple views for facial motion recording. They simplified the 3D reconstruction problem and assumed mirrors and the camera were vertical. Basu et al. [3] employed a front view and a mirrored view to capture 3D lip motion. In our previous work [20], we also applied mirrors for acquirement of facial images with different view directions. However, our 3D reconstruction algorithm proved simpler yet more accurate because it conveniently uses symmetric properties of mir-

rored objects. Readers can refer to [20] for a detailed explanation.

Some devices and research apply other concepts to estimate 3D motion or structure. Blanz et al. [6] used the optical flow method for correspondence recovery between scanned facial keyframes. Structured-light-based systems [11, 17, 29] project patterns onto a face and can therefore extract 3D shape and texture. Detailed undulation on a face surface can be captured with high-resolution cameras. Zhang et al.'s system [29] can even automatically track correspondences from consecutive depth images without markers by template matching and optical flow. However, the estimation can be unreliable for textureless regions.

3 Overview

3.1 Equipment setting

In order to enhance the distinctness of markers from others in video clips, we utilize the fluorescent phenomenon covering markers with fluorescent pigments. When illuminated by BLB lamps, the pigments are excited and emit fluorescence. Since the fluorescence belongs to visible light, no special attachment lens is required for the video camera. In our experiments, we found that fluorescent colors of our pigments could be roughly divided into four classes, green, blue, pink, and purple. To avoid ambiguity in the following tracking, we evenly place four classes of markers on a subject's face and keep markers as far as possible from those of the same color class.

The equipment setting of our tracking system is shown in Fig. 2. Two mirrors and two BLB lamps are placed in front of a digital video (DV) camcorder. The orientations and locations of mirrors can be arbitrary, as long as the front- and side-view images of a subject's face are covered by the camera's field of view (Fig. 3).

After confirming the camera's view field, including the frontal and two side views, the mirrors, the camera, and the intrinsic parameters of the camera have to be fixed. We use Bouguet's camera calibration toolbox (www.vision.caltech.edu/bouguetj/ calib_doc) based on Heikkila et al.'s work [16] to evaluate the intrinsic parameters (including focal lengths, distortion, etc.). The coordinate system is then normalized and undistorted based on the intrinsic parameters, called the normalized camera model. After this, we estimate the mirrors' parameters by our previous work [20]. The normalized coordinate system is applied to all the following steps.

Fig. 2. The tracking equipment. This photo is taken under normal light. Two "Blacklight Blue"(BLB) lamps are placed in front of a subject and mirrors. The low-cost special lamps are coated with fluorescent powders, and it can emit long wave UV-A radiation to excite luminescence

Fig. 3. A captured video clip of fluorescent markers illuminated only by BLB lamps. The fluorescence is visible in the visible light spectrum and no special lens is required for filtering

3.2 Initialization

Initialization of the tracking procedure reconstructs the 3D positions of markers in the first frame (the neutral face). To efficiently recover point correspondences in the first frame, two approaches can be used for different conditions.

The first approach is to employ 3D range scanned data. Figure 4 shows the process of recovering point correspondences. Before applying 3D scanned data, the coordinate system of the data must conform to the normalized camera model. First, markers' projected positions are extracted (Fig. 4a), and then a user has to manually select n

($n > 3$) corresponding point pairs on the nose tip, eye corners, mouth corners, etc. in the first video clip to form a 3D point set S_a. After corresponding feature points in 3D scanned data, S_b, are also designated, the affine transformation between 3D scanned data and specified markers' 3D structure can be evaluated by a least-squares solution proposed by Arun et al. [2].

While we extend the vector $\overrightarrow{op_i}$, where o is the camera's lens center and p_i the extracted projected position of marker i in the frontal view, the intersection of the line $\overrightarrow{op_i}$ and 3D scanned data is regarded as the 3D position of marker i, denoted as m_i. The corresponding point p_i' in a side view is then recovered by mirroring m_i to
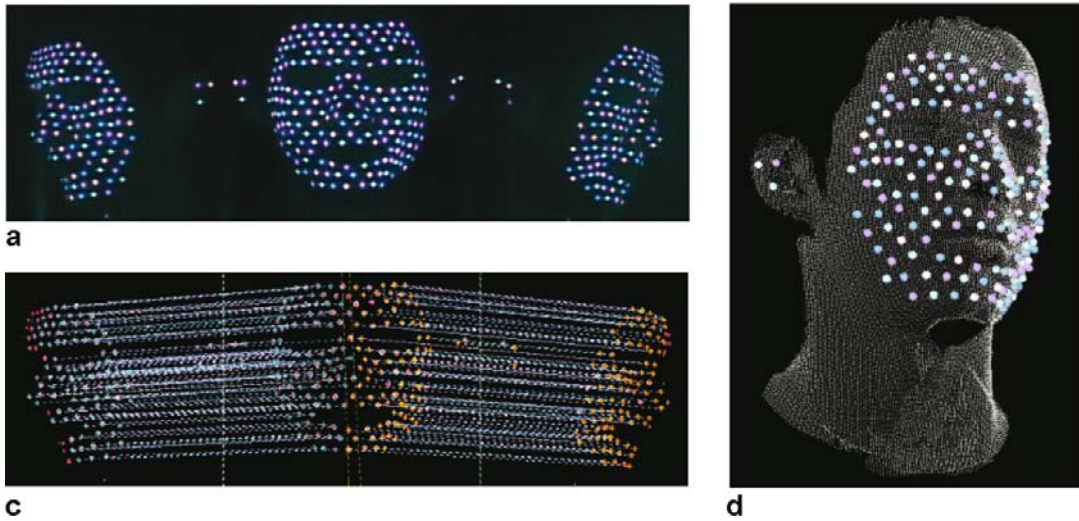

Fig. 4. Recovering 2D point correspondences with 3D scanned data and RBF interpolation

the mirrored space and projecting the mirrored one, m'_i, back to the image plane. Due to perturbation of measurement noise, within a tolerant region the nearest point of the same color class is regarded as the corresponding point p'_i.

The other approach is to recover point correspondences by evaluating a subject's 3D face structure directly from rigid-body motion. If an object is rigid or not deformable, affine transformation (rotation R and translation t) resulting from motion is equivalent to the inversed affine transformation resulting from changes in the coordinate system. Therefore, reconstructing the 3D structure from rigid-body motion is equivalent to reconstructing the 3D structure from multiple views [26]. A subject is required to retain his or her face in a neutral expression and slowly move his or her head in four directions: right-up, right-down, left-up, and left-down. A preliminary 3D structure of the face can be estimated from markers' projected motion in the frontal view, and point correspondence can then be recovered.

3.3 Overview of the tracking procedure

Figure 5 is the flow chart of the proposed tracking procedure. As mentioned in the Sect. 3.1, in the first step, we have to evaluate the parameters of the video camera and two mirrors. Markers' 3D positions in the neutral face are then estimated by the methods introduced in Sect. 3.2.

For each successive frame t ($t = 2 \ldots T_{end}$), feature extraction is first applied to extract markers' projected positions in the frontal and mirrored views. From the projected 2D positions in real-mirrored image pairs and mirror parameters, we can calculate a set of 3D positions, which are the markers' possible 3D positions. We call these 3D positions "potential 3D candidates" (Fig. 8). After this step, the tracking becomes a node-connection problem with the possibility of missing nodes.

Since we allow a subject's head to move naturally, we find that the head movement dominates the markers' motion trajectories. To avoid head motion seriously affecting the tracking results, before the "node matching" the global
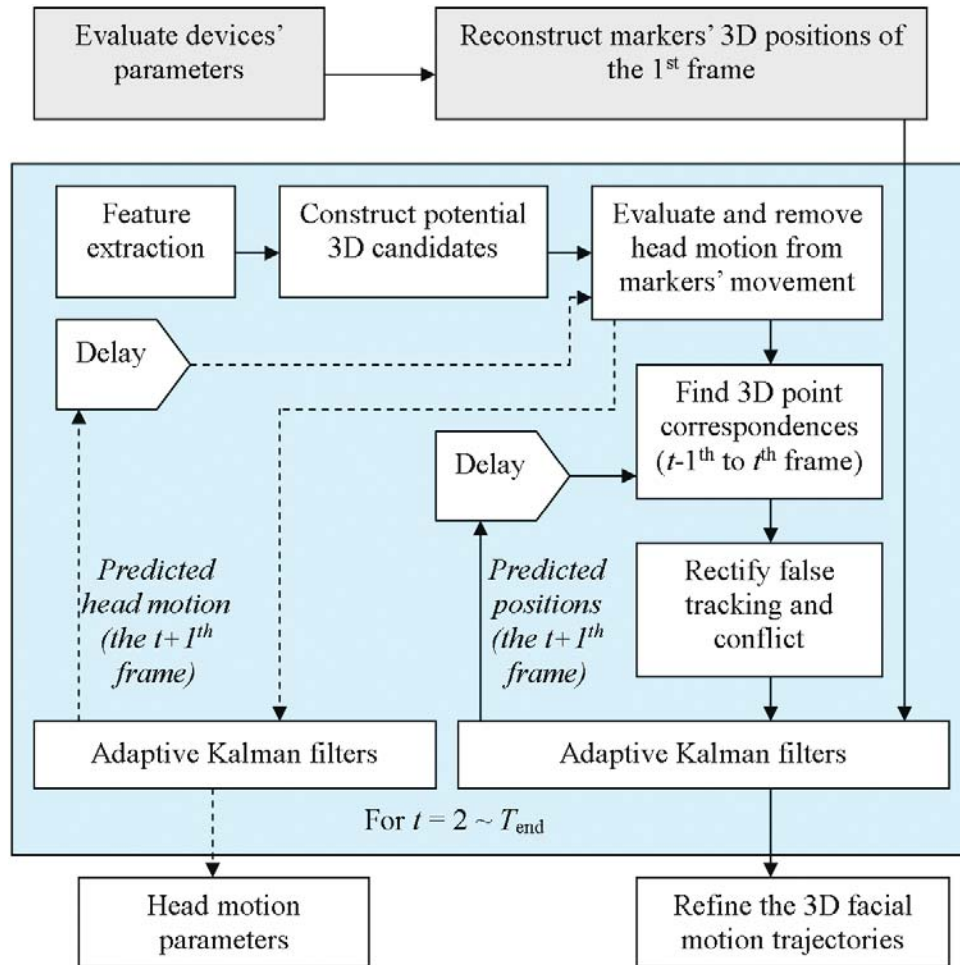

Fig. 5. The flow chart of our automatic 3D motion tracking procedure for dense UV-responsive markers

head motion has to be estimated and removed from 3D candidates. The head motion is estimated from a set of special markers, and adaptive Kalman filters, which work according to previous head motion transition, are applied to improve the stability.

After the head motion is removed from the 3D candidates, for each marker we take into account its previous trajectories and its neighbors' motion distribution to judge whether there is a most appropriate candidate or it is a missing-node situation. Once a marker belongs to a situation of missing node, false tracking, or tracking conflict, we apply the comprehensive information of spatial and temporal coherence to estimate the actual motion. Again, for each marker an individual Kalman filter is applied to improve the tracking stability.

Details of feature extraction and the generation of 3D candidates are described in Sect. 4. The tracking issues about head motion estimation, finding 3D point correspondences, and detection and rectification of tracking errors are then presented in Sect. 5.

4 Constructing 3D candidates from video clips

For efficiency of tracking, we first have to narrow the search space. This issue can be divided into two parts: extracting markers' projected 2D positions and constructing potential 3D candidates.

4.1 Extracting markers from video clips

As shown in the video clip (Fig. 3), because we use UV-responsive pigments and BLB lamps, markers are conspicuous in video clips. Hence, the automatic feature extraction can be more reliable and more feasible than under normal light conditions. We mainly follow the methodology of connected component analysis in computer vision, which is composed of thresholding, connected component labeling, and region property measurement, but we also slightly modify the implementation for computational efficiency.

Since the intensity of UV-responsive markers is much higher than that of other markers, to exclude pixels that have less probability of marker projection, the first stage is color thresholding. For efficiency, we skip the mathematical morphology operations used by many feature extraction systems. The thresholding works satisfactorily in most cases; the most troublesome case, interlaced scan lines, can be solved more efficiently by merging nearby connected components.

The second stage is color labeling. In our experiment, we collect six kinds of UV-responsive markers that are painted with pink, yellow, green, white, blue, and purple pigments. However, when illuminated by BLB lamps, there are only four typical colors—pink, blue-

green, dark blue, and purple. Hence, we mainly categorize markers into four color classes and each color class comprises dozens of color samples. A selection tool is provided to select these color samples from training videos. To classify the color of a pixel in video clips, the nearest neighborhood method (1-NN) is applied. To reduce the classification error resulting from intensity variation, the matching operation works on a normalized color space (nR, nG, nB), where $nR = \frac{R}{\sqrt{(R^2+G^2+B^2)}}$, $nG = \frac{G}{\sqrt{(R^2+G^2+B^2)}}$, $nB = \frac{B}{\sqrt{(R^2+G^2+B^2)}}$, and (R, G, B) is the original color value. In general, the more color samples in a color class, the more accurate the color classification of a pixel. For real-time or near-real-time applications, around four color samples in each color class are sufficient.

Connected component labeling is the third stage in our feature extraction. It groups connected pixels with the same color label number as a component, and we adopt 8-connected neighbors. In our case, a marker's projection is smaller than a radius of five pixels, and thus the process of connected component labeling can be simplified much more than general connected-component-labeling approaches. We modify the classical algorithm [15] as partial connected component labeling (PCCL). Unlike the classical algorithm, for each pixel (i, j) we take a one-pass process and check only its preceding neighbors, $(i-1, j-1)$, $(i, j-1)$, $(i+1, j-1)$, and $(i-1, j)$. Not all 8-connected components can be labeled as the same group by PCCL since we do not use a large equivalent class table for transiting label numbers as in the classical one. But the problem of inconsistent label numbers can easily be solved in our next stage.

After the process of partial connected component labeling, there are still redundant connected components caused by interlaced fields of video, incomplete connected component labeling, or noise. The fourth stage is to refine the connected components to make extracted components as close as possible to the actual markers' projection. Because markers are placed evenly on a face and the shortest distance between two markers of the same color class is longer than the diameter of a dot marker, nearby connected components should belong to the same marker. Therefore, the first two kinds of redundant connected components can be simply tackled by merging components with a distance less than the markers' average diameter. For the redundant components caused by noise, we suppress them by removing connected components less than four pixels.

4.2 Constructing 3D candidates by mirrored epipolar bands

If there are N_f and N_s feature points of a certain color class extracted in the frontal and side views respectively,

each point corresponding pair can generate a 3D candidate, and therefore there are a total of $N_f N_s$ 3D candidates of this color class. Guenter et al. [14] took all $N_f N_s$ potential 3D candidates to track N_{mrk} markers' motion, where N_{mrk} is the amount of actual markers, $N_{mrk} \ll N_f N_s$. However, in a two-view system, given a point p_i in the first image, its corresponding point is constrained to lie on a line called the "epipolar line" of p_i. With this constraint, one only has to search features along the epipolar line. The number of 3D candidates decreases substantially and the computation is much more efficient.

We found that there is a similar constraint in our mirror-reflected multiview structure. Since a mirrored view can be regarded as a flipped view from a virtual camera, the constraint should also exist but be flipped. We call this mirrored constraint the "mirrored epipolar line." We briefly introduce the concept of the mirrored epipolar line in Fig. 6. We assume that p is an extracted feature point, o the optic center, and p' the un-
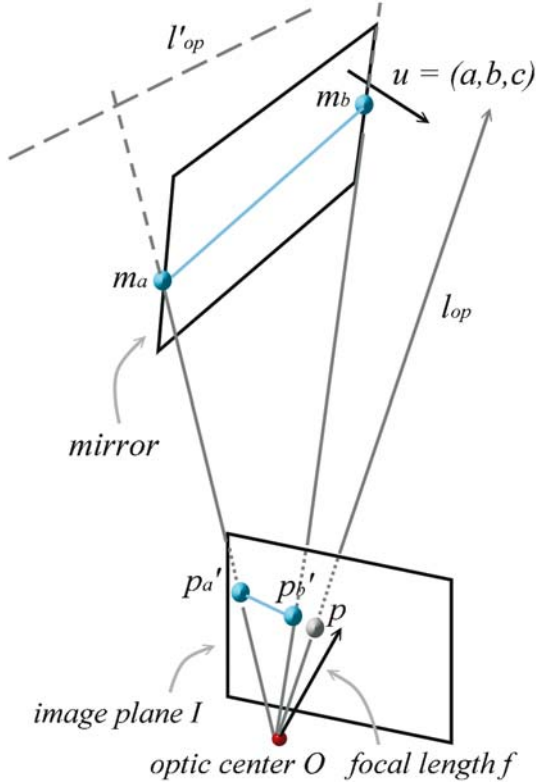

Fig. 6. A conceptual diagram of the mirrored epipolar line. p is an extracted feature in the frontal view and l_{op} is the line across o and p. l'_{op} is the line symmetric to l_{op} by the mirror plane. $\overline{m_a m_b}$ is the projection segment of l'_{op} on the mirror plane. $\overline{p'_a p'_b}$, the projection of $\overline{m_a m_b}$ on the image plane I, is the mirrored epipolar line segment of p

known corresponding point in the mirrored view. Since p is a projection, the actual marker's 3D position, m, must lie on the line l_{op}. According to the mirror symmetry property, the mirrored marker's 3D position, m', must lie on l'_{op}, which is a symmetric line of l_{op} with respect to the mirror plane. When a finite-size mirror model is adopted, the projection of l'_{op} is a line segment, and we denote it as $\overline{p'_a p'_b}$. The corresponding point p' must then lie on this mirrored epipolar line segment $\overline{p'_a p'_b}$, or otherwise the marker m is not visible in the mirrored view.

The mirrored epipolar line of a point p can easily be evaluated. In our previous work [20], we deduced an equation between point p, p' and a mirror's normal $u = [a, b, c]^T$:

$$(p')^T U p = 0, \quad \text{where} \quad U = \begin{bmatrix} 0 & -c & b \\ c & 0 & -a \\ -b & a & 0 \end{bmatrix}. \quad (1)$$

After we expand p and p' by their x, y, and z components, the equation becomes

$$\begin{bmatrix} x'_p & y'_p & 1 \end{bmatrix} \begin{bmatrix} -cy_p + b \\ cx_p - a \\ -bx_p + ay_p \end{bmatrix} = 0, \quad (2)$$

and the line

$$(-cy_p + b)x'_p + (cx_p - a)y'_p + (-bx_p + ay_p) = 0 \quad (3)$$

is the mirrored epipolar line of p.

For noise tolerance capability during potential 3D candidate evaluation, we extend the line k pixels up and down ($k = 1.5$ in our case) to form a "mirrored epipolar band" and search corresponding points of the same color class within the region between two constraint lines

$$(-cy_p + b)x'_p + (cx_p - a)y'_p + (-bx_p + ay_p) \\ + (cx_p - a)k = 0 \quad (3a)$$

and

$$(-cy_p + b)x'_p + (cx_p - a)y'_p + (-bx_p + ay_p) \\ - (cx_p - a)k = 0. \quad (3b)$$

Figure 7 shows an example of potential point corresponding pairs generated by the mirrored epipolar constraint; Fig. 8 shows the 3D candidates generated from the constrained point correspondences.

With this step the following tracking procedure can focus mainly on the set of potential 3D candidates. However, because there is measurement noise in extracted connected components and some markers are even occluded, the 3D candidates may not include all markers' positions. Therefore, an error-tolerant procedure has to be used for automatic tracking.
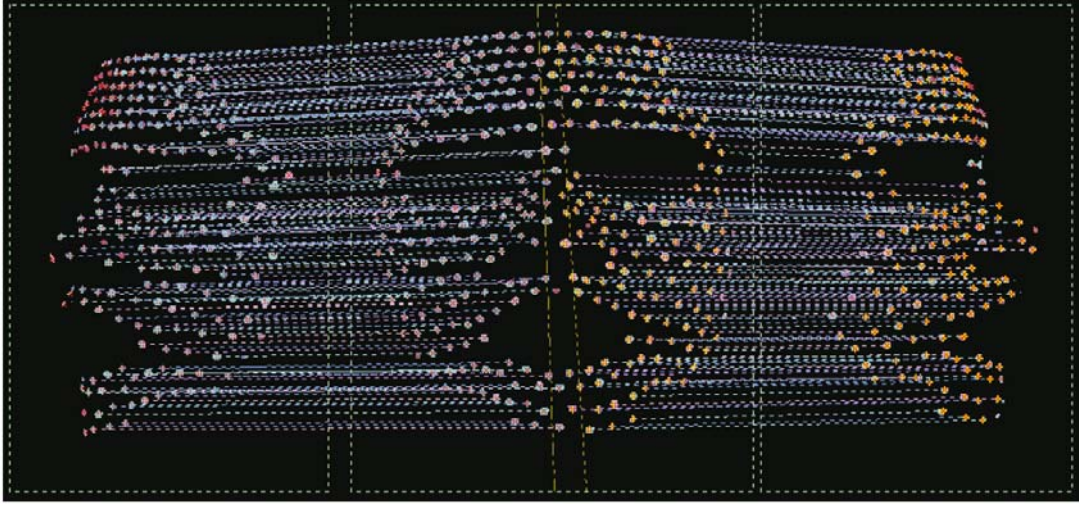
Fig. 7. Candidates of point corresponding pairs under mirrored epipolar constraints. For each extracted feature in the frontal view, each feature point of the same color that lies within its mirrored epipolar band is regarded as a corresponding point

Fig. 8. Potential 3D candidates generated under the mirrored epipolar constraint and the distance constraint. 3D candidates are first constructed from candidates of point correspondences; those whose positions are out of a bounding box are removed from the list of potential candidates

5 Reliable tracking

The 3D motion trajectories of markers comprise both facial motion and head motion. Because the moving range of a head is larger than that of facial muscles, when a subject enacts facial expressions and moves his or her head at the same time, most of the markers' motion results from head motion. This situation could result in the Kalman predictors and filters affected mainly by head motion. We adopt separate Kalman predictors/filters for head motion and facial motion tracking, and we find that the detection and rectification of tracking error are more reliable if head motion is removed in advance.

5.1 Head movement estimation and removal

We assume the head pose in the first frame ($t = 1$) is upright. We also define the head motion at time t as the affine transformation of the head pose at time t with respect to the head pose at $t = 1$. The relation can be represented as

$$h(t) = R_{head}(t) \cdot h(1) + T_{head}(t) , \qquad (4)$$

where h can be any point on a head irrelevant to facial motion, $R_{head}(t)$ is rotation, and $T_{head}(t)$ is translation. For automatic head movement tracking, seven specific markers are pasted on locations invariant to facial motion, such as a subject's ears and the concave tip on the nose column.

Adaptive Kalman filters are used to alleviate unevenness in trajectories resulting from measurement errors.

$R_{head}(t)$ and $T_{head}(t)$ both have three degrees of freedom. $T_{head}(t) = [t_x(t), t_y(t), t_z(t)]^T$. $R_{head}(t)$ is a 3×3 matrix and can be parameterized in terms of ($r_x(t)$, $r_y(t)$, and $r_z(t)$) in radians. Through least-squares fitting methods comparing elements of Eq. 5, ($r_x(t)$, $r_y(t)$, and $r_z(t)$) can be extracted from $R_{head}(t)$.

$$R_{head} = R_z R_y R_x$$
$$= \begin{bmatrix} \cos(r_z) & -\sin(r_z) & 0 \\ \sin(r_z) & \cos(r_z) & 0 \\ 0 & 0 & 1 \end{bmatrix} \begin{bmatrix} \cos(r_r) & 0 & \sin(r_y) \\ 0 & 1 & 0 \\ -\sin(r_y) & 0 & \cos(r_r) \end{bmatrix} \begin{bmatrix} 1 & 0 & 0 \\ 0 & \cos(r_x) & -\sin(r_x) \\ 0 & \sin(r_x) & \cos(r_x) \end{bmatrix}$$
$$= \begin{bmatrix} c(r_z)c(r_y) & -s(r_z)c(r_x)+c(r_z)s(r_y)s(r_x) & s(r_z)s(r_x)+c(r_z)s(r_y)s(r_x) \\ s(r_z)s(r_y) & c(r_z)c(r_x)+s(r_z)s(r_y)s(r_x) & -c(r_z)s(r_x)+s(r_z)s(r_y)s(r_x) \\ -s(r_y) & c(r_y)s(r_x) & c(r_y)c(r_x) \end{bmatrix}$$
$$\tag{5}$$

where R_z, R_y, and R_x are rotation matrices along the z-, y-, and x-axes; $c()$ and $s()$ are abbreviations of $\cos()$ and $\sin()$. Kalman filters are applied directly to these six parameters: $[r_x(t), r_y(t), r_z(t), t_x(t), t_y(t), t_z(t)]$. The process of head motion evaluation is as follows. We use $r_x(t+1|t)$ to represent the prediction of parameter r_x at time $t+1$ based on previous data of $r_x(1)$ to $r_x(t)$; similarly for other parameters.

Step 1. Designate specific markers s_i (for $i = 1 \ldots N_{smrk}$, where N_{smrk} is the amount of specific markers, $N_{smrk} = 7$ in our case) for head motion tracking from the reconstructed 3D markers of the neutral face ($t = 1$), and denote their positions as $ms_i(1)$. (Either a specific color is used for the special markers or users have to designate them in the first frame.)

Step 2. Initialize parameters of adaptive Kalman filters and set $r_x(1) = r_y(1) = r_z(1) = 0$, $t_x(1) = t_y(1) = t_z(1) = 0$, and $t = 1$.

Step 3. Predict the head motion parameters $r_x(t+1|t)$, $r_y(t+1|t)$, $r_z(t+1|t)$, $t_x(t+1|t)$, $t_y(t+1|t)$, and $t_z(t+1|t)$ by Kalman predictors and then construct $R_{head}(t+1|t)$ and $T_{head}(t+1|t)$ by Eq. 5. Increase timestamp $t = t + 1$

Step 4. Generate predicted positions of specific markers as

$$ms_i(t|t-1) = R_{head}(t|t-1) \times ms_i(1) + T_{head}(t|t-1) \tag{6}$$

and find $ms_i(t)$ by searching the nearest potential 3D candidates of the same color. The search is restricted within a distance d_{srch} from $ms_i(t|t-1)$. If no candidate is found, set the marker as invalid at time t.

Step 5. Detect tracking error: if estimated motions are abnormal when compared to other specific markers, then set the markers of odd estimation as invalid at time t.

(The tracking error detection is presented in the next subsection; we skip the details here.)

Step 6. Estimate the affine transformation (R_{msr} and T_{msr}) of valid specific markers between time t and the first frame by the method proposed by Arun et al. [2].

Step 7. Extract $r_{msr\_x}(t)$, $r_{msr\_y}(t)$, and $r_{msr\_z}(t)$ from R_{msr} by Eq. 5 and extract $t_{msr\_x}(t)$, $t_{msr\_y}(t)$, and $t_{msr\_z}(t)$ from T_{msr}.
Take the extracted parameters as measurement inputs to the adaptive Kalman filter and estimate the output $[r_x(t), r_y(t), r_z(t), t_x(t), t_y(t), t_z(t)]$.

Step 7. If $t > T_{limit}$, stop; else go to *Step 3*.

We use a position-velocity configuration for the Kalman filters for translation, where 3D positions are measurement input and the internal states are positions and velocities. The operation of the Kalman filters for rotation is similar, but the input is a set of angles and the internal states represent angles and angular velocities. Once the head motion at time t is evaluated, an inverse affine transformation is applied to all 3D candidates for head motion removal.

5.2 Recovering frame-to-frame 3D point correspondence with outlier detection

In this subsection, we assume that head motion is removed from potential 3D candidates, and our goal is to track markers' motion trajectories from a frame-by-frame sequence of potential 3D candidates. Figure 9 is a conceptual diagram of the problem statement. For clarity of explanation, we take the situation of only one color class of markers as examples. The methodology of processing each color class independently can extend to cases of multiple color classes.

The number of potential 3D candidates in a frame is around $1.2 \sim 2.3$ times the number of the actual markers. The additional 3D candidates can be regarded as false detection in the multitarget tracking problem. If only false detection occurs, the graph algorithms for minimum cost network flow (MCNF) can evaluate the optimal solution. In our case, we employ Kalman predictors and filters to efficiently calculate the time-varying position variation of each marker. However, a marker can "miss" in video clips occasionally. The missing condition results from blocking or occlusion due to camera views, incorrect classification of marker colors, or noise disturbance. When the missing and false detection occur concurrently, a simple tracking method without evaluation of tracking error would degenerate and the successive motion trajectories could be disordered.

We use an example to explain the serious consequence of tracking errors. In Fig. 10, marker **B** is not included in the potential 3D candidates of the third frame, and its actual position is denoted as **B**(3). Based on the previous trajectory, **B'**(3) is the nearest potential candidate with
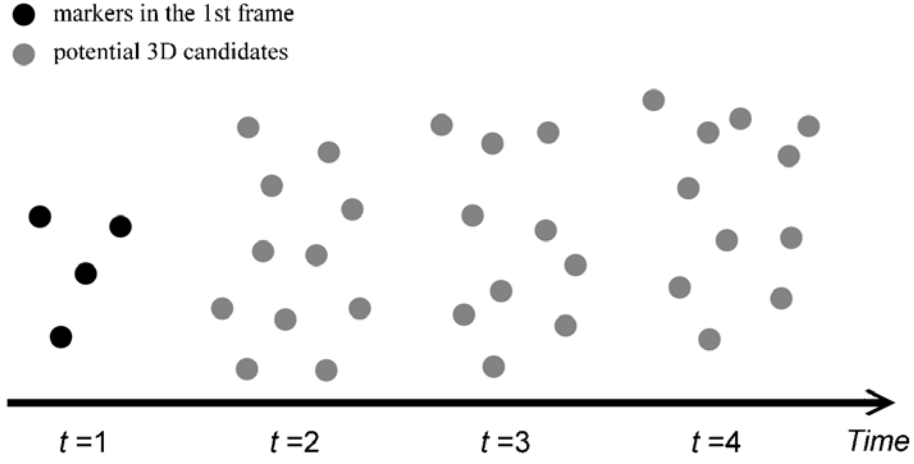
Fig. 9. A conceptual figure for the problem statement of 3D marker tracking. The markers' 3D positions in the 1st frame are first evaluated. The goal of 3D motion tracking is to find frame-to-frame 3D point correspondences from sequences of potential 3D candidates
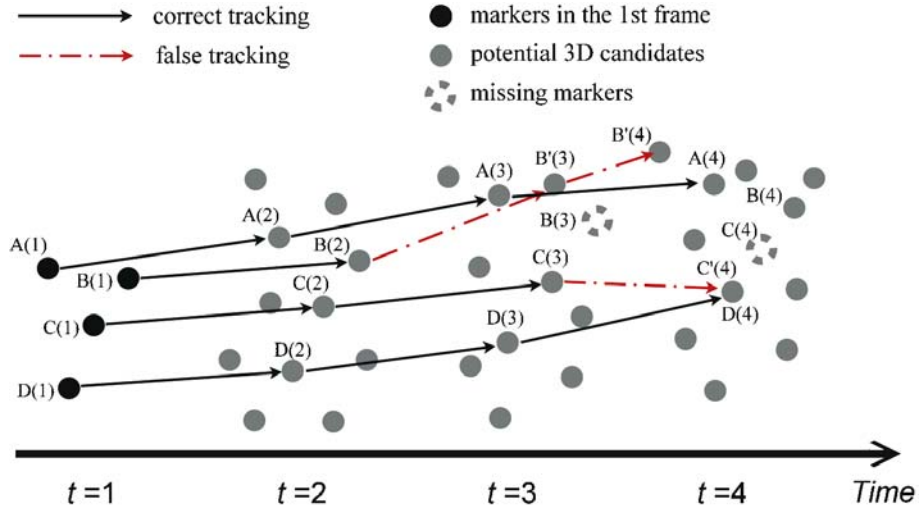

Fig. 10. An example of tracking errors resulting from missing markers

respect to the predicted position. According to this false trajectory $\mathbf{B}(1) \rightarrow \mathbf{B}(2) \rightarrow \mathbf{B'}(3)$, the next position should be $\mathbf{B'}(4)$. Consequently, the motion trajectory starts to "derail" seriously and is difficult to recover. Furthermore, false tracking of a marker may even interfere with tracking of other markers. In the example of Fig. 10, marker $\mathbf{C}$ is also undetected in the fourth frame; the nearest candidates with respect to the predicted position is $\mathbf{C'}(4)$. Unfortunately, $\mathbf{C'}(4)$ is actually marker $\mathbf{D}$ at the fourth frame, denoted as $\mathbf{D}(4)$. Because each potential candidate should be "occupied" by one marker at most, a misjudgment would not only make marker $\mathbf{C}$ but also marker $\mathbf{D}$ depart from the correct trajectories.

For detection of tracking errors, we take advantage of the spatial coherence of face surfaces, which means a marker's motion is similar to that of its neighbors. Be-

fore we present our method, the terms are specified in advance. For a marker i, its neighbors are other markers that locate within a 3D distance ε from its position in the neutral face, $m_i(1)$. For the motion of marker i at time t, we do not use the 3D location difference between time $t-1$ and t but instead use the location difference between time t and time 1. We denote $v_i(t) = m_i(t) - m_i(1)$; this is because the former is easily disturbed by measurement noise but the latter is less sensitive to noise. The motion similarity between marker i and marker j at time t is defined as the Euclidean distance between two motion vectors $\|v_i(t) - v_j(t)\|$.

A statistical approach is used to judge whether a marker's motion at time t is a tracking error. For each marker i, we first calculate the similarity of each neighbor and sort them in decreasing order. To avoid contamination of the

judgment by unknown tracking error of neighbors, only the first α% neighbors in order of similarity are included in the sample space Ω ($\alpha = 66.67$ in our experiments). This mechanism can also solve the judgment problem on discontinuous parts (e.g., excluding motions on the upper lips from the reference neighbor sets of motions on the lower lips). We presume that the vectors within the sample space Ω approximate a Gaussian distribution. The averages and standard deviations of the x, y, and z components of v_j (for all $j \in \Omega$) are denoted as $(\mu_{vx}, \mu_{vy}, \mu_{vz})$ and $(\sigma_{vx}, \sigma_{vy}, \sigma_{vz})$, respectively. We define that a tracked motion $v_i(t)$ is valid if it is not far from the distribution of most of its neighbors.

The judgment criterion of valid or invalid tracking for the marker i is

$$\begin{cases} JF(i, t) \leqslant threshold, & \text{valid tracking} \\ \text{else,} & \text{invalid tracking} \end{cases} \tag{7}$$

and the judgment function is

$$JF(i, t) = \sqrt{S_x^2 + S_y^2 + S_z^2}, \tag{8}$$

where $S_x = \frac{x_{vi} - \mu_{vx}}{\sigma_{vx} + k}$, $S_y = \frac{y_{vi} - \mu_{vy}}{\sigma_{vy} + k}$, $S_z = \frac{x_{vi} - \mu_{vz}}{\sigma_{vz} + k}$, and $v_i(t) = (x_{vi}, y_{vi}, z_{vi})$.

S_x, S_y, and S_z can be regarded as the divergence of v_i with respect to the refined neighbors Ω in the x, y, and z directions. If the difference between v_i and the average of its neighbors is within the standard deviations, the values S are smaller than 1; on the other hand, if the divergences are larger, the values increase. In Eq. 8, k is a small user-defined number. With k in the denominators, we can prevent unpredictable values of S_x, S_y, and S_z when markers are close to their locations of the neutral face.

After we eliminate the invalid tracking of 3D candidates, a conflicting situation can still exist. Two valid motions that do not share the same 3D candidates could have the same extracted 2D feature points in either the frontal view or the side view. We call this the tracking conflict. To prevent the tracking conflict, we simply evaluate the number of valid motions for each 2D feature point. If a 2D feature point is "occupied" by more than one valid motion, we only keep the motion closest to the prediction as a valid motion.

5.3 Estimating positions of missing markers

If an invalid tracking is detected, the similarity of its neighbors in motion can also be used to conjecture the position or motion of the missing marker. Based on this idea, two interpolation methods are applied to the estimation. The first one is the weighted combination method. For a missing marker i, the motion at time t can be estimated by a weighted combination of that of its neighbors and it can be presented by the equation:

$$v_i = \sum_j \left(\frac{1}{d_{ij} + kc} \right) v_j, \quad \text{for } j \in \text{Neighbor}(v_i), \tag{9}$$

where d_{ij} is the distance between m_i and m_j in the neutral face and kc is a small constant to avoid a very large weight when the marker i and j are quite close in the neutral face.

In addition, a radial-basis-function (RBF) based data scattering method is also appropriate for the position estimation of missing markers. The abovementioned weighted combination method tends to average and smooth the motions of all the neighbors; in contrast, the
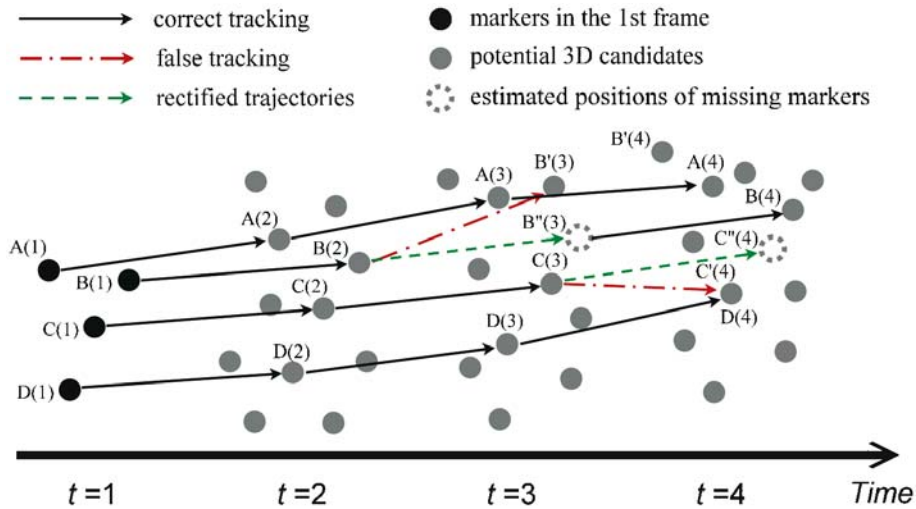

Fig. 11. The rectified motion trajectories. We utilize the temporal coherence of a marker's motion and the spatial coherence between neighbor markers to detect and rectify false tracking
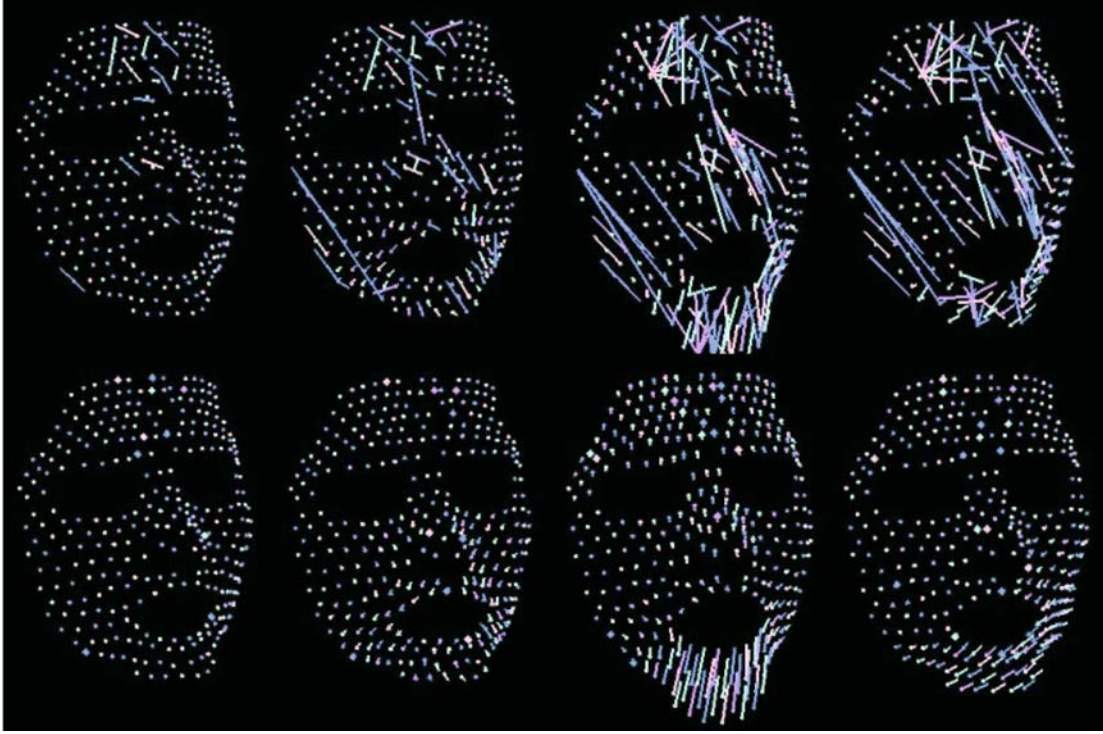
Fig. 12. The tracking results without vs. with tracking error rectification. The upper part is the result tracked without false tracking detection; the lower part is the result tracked with our rectification method. The snapshots from left to right are captured at $t = 20, 100, 300$ and 500

influence of nearby neighbors can be greater in RBF interpolation in general (it depends on the radial basis function), and, therefore, more prominent motions can be estimated. Since the RBF interpolation is more time consuming, the weighted combination is adopted for real-time or near-real-time tracking. Figure 11 shows a conceptual diagram of rectifying false tracking; Fig. 12 shows the tracking results by a method with Kalman filtering only and by our method with rectification of tracking error.

6 Experimental results and discussion

Using the method proposed in this paper, we have successfully captured a large amount of dense facial motion data from three subjects, including two males and one female. On one male subject's face we placed 320 markers 3 mm in diameter; on the other two subjects' faces we placed 196 markers 4 mm in diameter and 7 special markers for head motion tracking. Due to view limitations and measurement errors, a small amount of markers are not visible in at least two views in half of the video sequence. Only 300 markers are actually tracked in the former case, 179 and 188 markers in the later ones.

In our experiments, motion that we intended to capture consists of three parts: coarticulations of visual speech

(motion transition between phonemes), facial expressions, and natural speech. Regarding coarticulations, each of the subjects was required to pronounce 14 MPEG-4 basic phonemes, also called visemes. They are "none," "p," "f," "T," "t," "k," "tS," "s," "n," "r," "A:," "e," and "i." Besides these, the subjects were also required to pronounce several vowel–consonant, vowel–vowel words, such as "tip," "pop," "void," etc. Concerning facial expressions, subjects were required to perform 6 MPEG-4 facial expressions comprising "neutral," "joy," "sadness," "anger," "fear," "disgust," and "surprise." Also, they had to perform several exaggerated expressions, e.g., mouth pursing, mouth twisting, cheek bulging, etc. Lastly, they were asked to speak about three different topics. Each of these talks was more than 1.5 min (2700 frames) and accompanied with vivid facial expressions. In the case without special markers for head motion estimation, the subjects' head is fixed; in the other cases, subjects can freely and naturally nod or shake their heads while speaking.

On a 3.0-GHz Pentium 4 PC, our system can automatically track motion trajectories of 300 markers at a speed of 9.2 fps. It can track 188 markers with head motion estimation at a speed of 12.75 fps.

For analysis, we calculate the occurrence of tracking errors. As we mentioned in previous sections, we divide the tracking errors into three categories: missing nodes, false tracking, and tracking conflicts. Since our detection
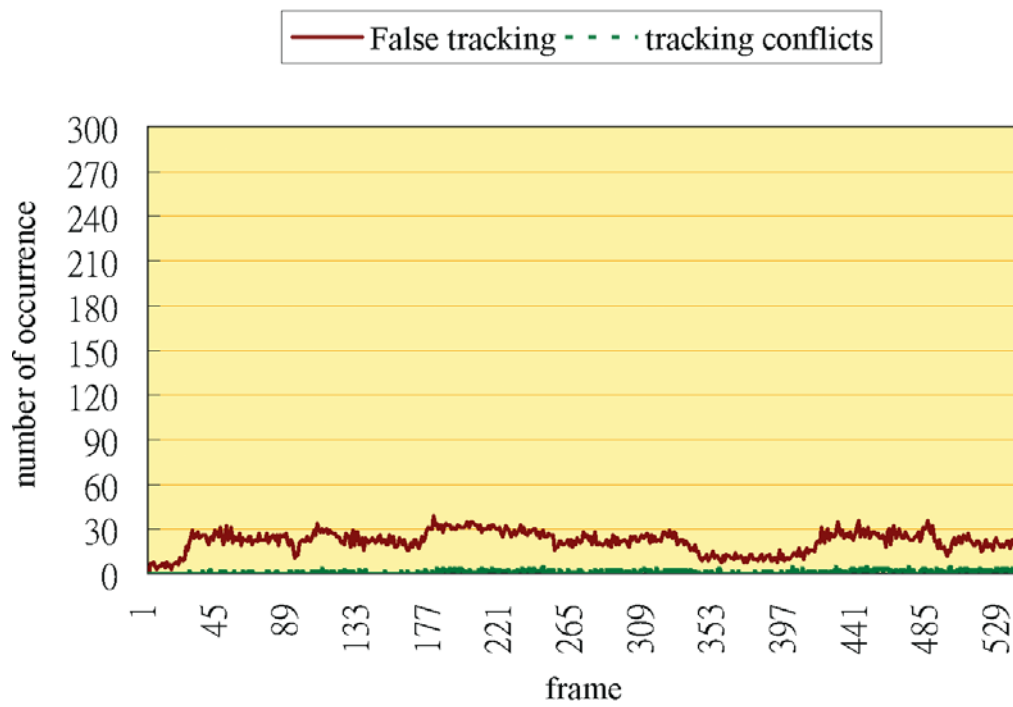
Fig. 13. Numbers of tracking errors detected in each frame of the same video sequence of Fig. 12
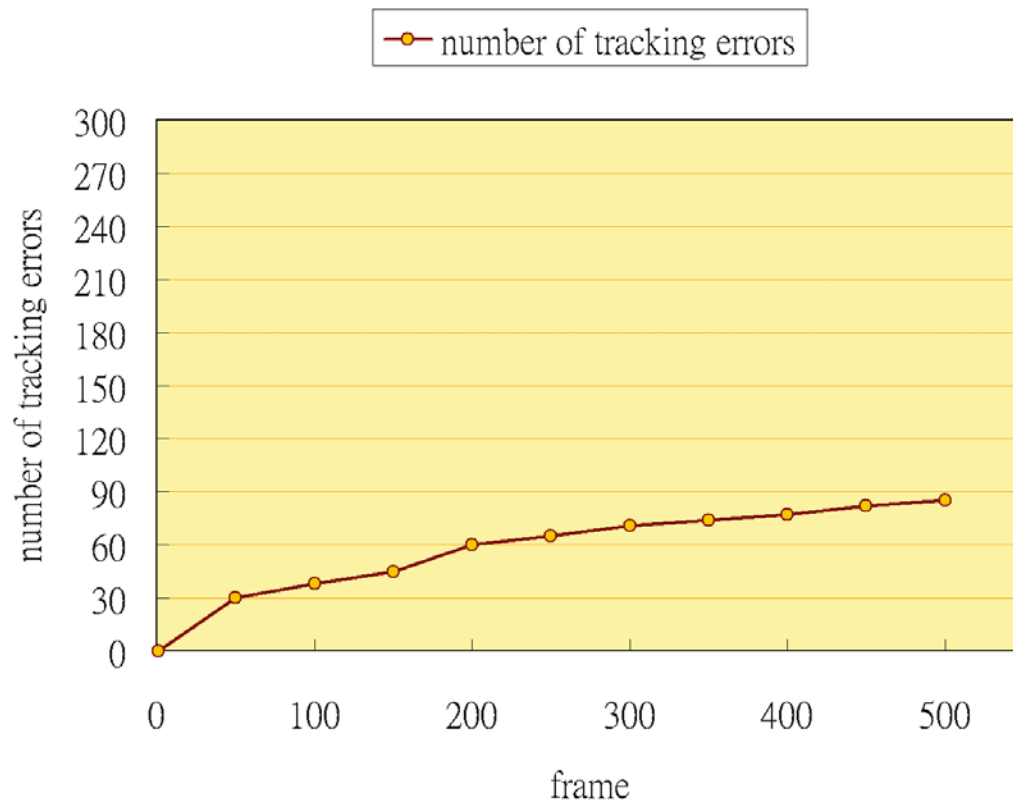

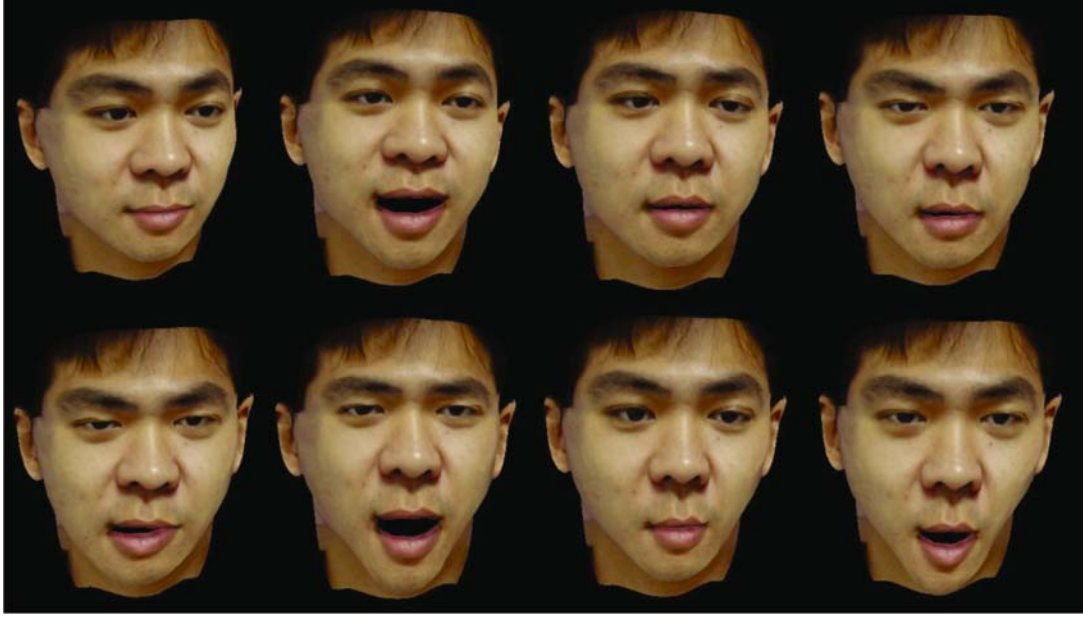**Fig. 14.** The number of accumulated tracking errors while no rectification is applied

Fig. 15. Synthetic subtle facial expressions of joy, sadness, anger, fear, and disgust.

Fig. 16. Synthetic facial expressions of pronouncing "a-i-u-e-o"

and management processes for missing nodes and false tracking are the same, we merge them into a single state: false tracking. Occurrence of tracking errors usually results from abrupt facial motion and is quite divergent in different video sequences.

For instance, we take a video sequence (Fig. 12) where a subject performed exaggerated facial expressions. As shown in Fig. 13, the average percentage of false tracking in each frame is about 7.45%, and the average percentage of tracking conflicts, which excluded the false tracking, is about 0.34%. The percentage is small, but if the tracking errors are not detected and rectified automatically, they

can accumulate frame by frame and the tracking results can degenerate dramatically as time passes. The upper part of Fig. 12 shows the disaster of tracking without rectification. As shown in the lower part of Fig. 12, with our proposed method we can retain tracking stability and accuracy. The number of tracking errors that occur in the upper part of Fig. 12 is shown in Fig. 14. Without rectification, almost one third of markers fall within the tracking errors.

The tracking results have also been applied to our real-time facial animation system [20]; the results are shown in Figs. 15–17. The static images may not manifest the time course reconstruction quality in tracking or motion retar-

Table 1. The distribution of CPU usages in our system

Operation	CPU usage
DV AVI file decoding	28.2%
Image processing (labeling, connected components, etc.)	29.9%
Calculating 3D candidates	18.0%
Finding best trajectories	23.9%

Fig. 17. Applying captured facial expressions to others' face models

geting. Demo videos are available on our project Web site listed in the conclusion.

As shown in Table 1, there is no obvious bottleneck stage of the CPU usage in our system. However, the operations in the stages of image processing and calculating 3D candidate points are mostly parallel, which can be further improved by SIMD (single instruction multiple data) or parallel computing.

7 Conclusion and future work

In this paper, we propose a new tracking procedure to automatically capture dense facial motion parameters from mirror-reflected multiview video, employing the property of mirror epipolar bands to rapidly generate 3D candidates and effectively utilizing the spatial and temporal coherence of dense facial markers to detect and rectify tracking errors. Our system can efficiently track such numerous

motion trajectories in near real time. Moreover, our procedure is a general method and could also be applied to track motion of other continuous surfaces.

All equipment used in the proposed system is off the shelf and inexpensive. This system can significantly lower the entry barrier for research about analysis and synthesis of facial motion. Our demonstrations are now downloadable at our project website: `http://www.cmlab. csie.ntu.edu.tw/~ichen/MFAPExt/MFAPExt _Intro.htm`. Besides the demonstrations, an executable software package, user instructions, and examples are also on the Web site for users to download for their own research.

Currently, the tracked motion parameters have been applied to our facial animation system. Dense facial motion data can be further used for refining coefficients of existing facial motion models and even a criterion for face surface analysis. In our future work, we plan to analyze the correlations of facial surface points, for example, finding out which marker sets are the most representative.

Table 2. The initial values of internal states' parameters in adaptive Kalman filters. (1 *frame* = 1/29.97 sec)

State	Variance of measurement noise	Variance of velocity change
x_{mi}	1.69 mm^2	21.87 $(mm/frame)^2$
y_{mi}	1.69 mm^2	78.08 $(mm/frame)^2$
z_{mi}	3.31 mm^2	35.10 $(mm/frame)^2$
r_x	0.684 $degree^2$	43.77 $(degree/frame)^2$
r_y	0.858 $degree^2$	24.62 $(degree/frame)^2$
r_z	0.985 $degree^2$	2.736 $(degree/frame)^2$
t_x	1.00 mm^2	27.00 $(mm/frame)^2$
t_y	1.00 mm^2	27.00 $(mm/frame)^2$
t_z	1.56 mm^2	27.00 $(mm/frame)^2$

8 Appendix

We adapt a position-velocity configuration for the Kalman filters. Users can refer to [4] for the detailed state transition and system equations. The noise parameters are dynamically adaptable according to prediction errors. The inital values of the parameters of feature point $m_i = (x_{mi}, y_{mi}, z_{mi})$, head rotation (r_x, r_y, r_z), and head translation (t_x, t_y, t_z) are defined empirically as listed in Table 2.

References

1. Ahlberg J (2002) An active model for facial feature tracking. EURASIP J Appl Signal Process 6:566–571
2. Arun KS, Huang TS, Blostein SD (1987) Least square fitting of two 3D point sets. IEEE Trans Pattern Anal Mach Intell 9(5):698–700
3. Basu S, Pentland A (1997) A three-dimensional model of human lip motions trained from video. In: Proceedings of the workshop on IEEE non-rigid and articulated motion, San Juan, Puerto Rico, pp 46–53
4. Bozic SM (1979) Digital and Kalman filtering. Edward Arnold, London
5. Blanz V, Vetter T (1999) A morphable model for the synthesis of 3D faces. In: Proceedings of ACM SIGGRAPH'99, pp 353–360
6. Blanz V, Basso C, Poggio T, Vetter T (2003) Reanimating faces in images and video. Comput Graph Forum 22(2):641–650
7. Brand M (1999) Voice puppetry. In: Proceedings of SIGGRAPH'99, pp 21–28
8. Buckley K, Vaddiraju A, Perry R (2000) A new pruning/merging algorithm for MHT multitarget tracking. In: Proceedings of Radar-2000
9. Castañon DA (1990) Efficient algorithms for finding the k best paths through a trellis. IEEE Trans Aerospace Elect Syst 26(1):405–410
10. Cohen MM, Massaro DW (1993) Modeling co-articulation in synthetic visual speech. In: Magnenat-Thalmann N, Thalmann D (eds) Models and techniques in computer animation. Springer, Berlin Heidelberg New York, pp 139–156
11. Davis J, Nehab D, Ramamoorthi R, Rusinkiewicz S (2005) Spacetime stereo: a unifying framework for depth from triangulation. IEEE Trans Pattern Anal Mach Intell 27(1):296–302
12. Ezzat T, Geiger G, Poggio T (2002) Trainable videorealistic speech animation. ACM Trans Graph 21(2):388–398 (also in Proceedings of SIGGRAPH'02)
13. Goto T, Kshirsagar S, Magnenat-Thalmann N (2001) Automatic face cloning and animation using real-time facial feature tracking and speech acquisition. IEEE Signal Process Mag 18(2):17–25
14. Guenter B, Grimm C, Wood D, Malvar H, Pighin F (1998) Making faces. In: Proceedings of ACM SIGGRAPH'98, pp 55–66
15. Haralick RH, Shapiro LG (1992) Computer and robotic vision, vol 1. Addison-Wesley, Reading, MA
16. Heikkilä J, Silvén O (1997) A four-step camera calibration procedure with implicit image correction. In: Proceedings of the IEEE conference on computer vision and pattern recognition, San Juan, Puerto Rico, pp 1106–1112
17. Kalberer GA, Gool LV (2001) Face animation based on observed 3D speech dynamics. In: Proceedings of Computer Animation 2001, Seoul, Korea. IEEE Press, New York, pp 18–24
18. Kuratate T, Yehia H, Vatikiotis-Bateson E (1998) Kinematics-based synthesis of realistic talking faces. In: Proceedings of Auditory-Visual Speech Processing, pp 185–190
19. Kshirsagar S, Magnenat-Thalmann N (2003) Visyllable based speech animation. Comput Graph Forum 22(2):631–639
20. Lin I-C, Yeh J-S, Ouhyoung M (2002) Extracting 3D facial animation parameters from multiview video clips. IEEE Comput Graph Appl 22(6):72–80
21. Pandzic IS, Ostermann J, Millen D (1999) User evaluation: synthetic talking faces for interactive services. Visual Comput 15:330–340
22. Patterson EC, Litwinowicz PC, Greene N (1991) Facial animation by spatial mapping. In: Proceedings of Computer Animation '91. Springer, Berlin Heidelberg New York, pp 31–44
23. Pighin F, Hecker J, Lischinski D, Szeliski R, Salesin DH (1998) Synthesizing realistic facial expressions from photographs. In: Proceedings of ACM SIGGRAPH '98, pp 75–84
24. Pighin F, Szeliski R, Salesin DH (1999) Resynthesizing facial animation through 3D model-based tracking. In: Proceedings of the international conference on computer vison, 1:143–150
25. Tu P-H, Lin I-C, Yeh J-S, Liang R-H, Ouhyoung M (2004) Surface detail

capturing for realistic facial animation. J Comput Sci Technol 19(5):618–625
26. Weng J, Huang TS, Ahuja N (1989) Motion and structure from two perspective views: algorithms, error analysis, and error estimation. IEEE Trans Pattern Anal Mach Intell 11(5):451–476
27. Wolf JK (1989) Finding the best set of K paths through a trellis with application to multitarget tracking. IEEE Trans Aerospace Elect Syst 26(1):287–296
28. Yeasin M, Polat E, Sharma R (2004) A mutiobject tracking framework for interactive mutimedia applications. IEEE Trans Multimedia 6(2):398–405
29. Zhang L, Snavely N, Curless B, Seitz SM (2004) Spacetime faces: high resolution capture for modeling and animation. ACM Trans Graph 23(2):548–558 (also in Proceedings of SIGGRAPH'04)

I-CHEN LIN is an assistant professor in the Department of Computer and Information Science, National Chiao Tung University, Taiwan. His research interests include computer graphics and virtual reality, especially in facial animation, motion capture, and 3D object modeling. He received a B.S. and a Ph.D. in computer science from National Taiwan University in 1998 and 2003, respectively. He is a member of ACM SIGGRAPH, IEEE, and IEEE Computer Society.

MING OUHYOUNG is a professor in the Graduate Institute of Networking and Multimedia and in the Department of Computer Science and Information Engineering, National Taiwan University. His research interests include computer graphics, virtual reality and multimedia systems. He received a B.S. and an M.S. in electrical engineering from National Taiwan University and a Ph.D. from the University of North Carolina at Chapel Hill. He is a member of IEEE and ACM.